Dispersion-Driven Morphology of Mechanically Confined Polymer Films

K. Dalnoki-Veress, B. G. Nickel, and J. R. Dutcher*

Department of Physics and the Guelph-Waterloo Program for Graduate Work in Physics, University of Guelph, Guelph, Ontario, Canada N1G 2W1

(Received 12 May 1998)

To probe the effects of mechanical confinement on freely standing polystyrene (PS) films, we have symmetrically capped freely standing PS films by thin, solid layers. Annealing of the trilayer films produces a novel lateral morphology which is driven by the dispersion force between the capping layers. A simple model is presented which describes the scaling behavior of the morphology with the layer thicknesses. The same morphology is observed for freely standing and supported films in eight different systems. We also demonstrate reversibility of the morphology by manipulation of the dispersion force. [S0031-9007(99)08501-4]

PACS numbers: 68.15.+e, 68.55.Jk, 68.60.Dv

Confinement of polymer molecules on length scales comparable to the size of the molecules can affect their physical properties, such as chain conformation and mobility ([1], and references therein, and [2–5]), and processes, such as phase separation ([6], and references therein). The nature of the interaction between the polymer molecules and the confining material determines the thermal stability of the confined molecules. In the absence of mechanical confinement, thermal instability of thin polymer films can lead to dewetting of films supported on substrates [7–9] and hole formation in freely standing films [10,11]. This instability is due to the long-range, attractive van der Waals or dispersion force [12] which amplifies thermal fluctuations of the interfaces. This is the mechanism responsible for the bursting of, for example, soap films [13,14]. The control of this instability creates possibilities for unique self-assemblies of polymer molecules on surfaces patterned on submicron length scales.

In this Letter, we describe our investigation of the thermal stability of freely standing *trilayer* films in which a thin polymer layer has been capped on both film surfaces with thin, solid capping layers. As expected, the presence of the capping layers prevents the formation of holes that was observed for freely standing polystyrene (PS) films at elevated temperatures [11]. Surprisingly, aggressive annealing of the trilayer films, containing a single layer of homopolymer, results in a novel in-plane structure (lateral morphology) similar to that observed for polymer blend films [6]. In the present case, the morphology transformation is driven not by a phase separation process [6] but rather by the instability due to the attractive dispersion force between the capping layer-air surfaces. We present a simple model that describes the dependence of the morphology on the polymer and capping layer thicknesses and verify the generality of the instability by the observation of the same morphology in eight different freely standing and supported film systems. For one of these systems we demonstrate reversibility of the morphology by manipulation of the dispersion force, providing a sensitive probe of one of the fundamental forces which govern self-assembly of materials at very small length scales. The ability to tune the morphology by controlling various experimental parameters suggests potential uses for these systems as, e.g., sensors or templates for the preparation of patterned surfaces [15].

We describe in detail the case of freely standing trilayer films consisting of a PS film of thickness h symmetrically capped with silicon oxide (SiO_x) layers, each of thickness L (SiO_x-PS-SiO_x). Monodisperse ($\overline{M}_w/\overline{M}_n = 1.11$), high molecular weight ($\overline{M}_w = 767 \times 10^3$) PS obtained from Polymer Source Inc. was dissolved in toluene. Polystyrene films ($30 < h < 121$ nm) were made by spincoating the solutions (4000 rpm) onto clean glass slides. The samples were annealed under vacuum at $T = 110\,^\circ\mathrm{C}$ for 12 h to remove residual solvent and cooled at $1\,^\circ\mathrm{C/min}$ to room temperature. Freely standing PS films were created by using a water transfer technique to place the PS films over a 4-mm-diameter hole in a stainless steel holder [1]. Pieces of the same PS films were also transferred onto clean Si wafers for PS film thickness determination using ellipsometry.

To create freely standing trilayer films, we evaporated thin layers of SiO_x onto both sides of the freely standing PS films. We chose SiO_x as the capping layer material because it remains solid during the annealing procedure described below and sharp SiO_x-PS interfaces are obtained [1,6,16]. In the evaporator, the ambient pressure was 1×10^{-6} torr, and the pressure during evaporation was $(1–2) \times 10^{-5}$ torr. To limit heating of the PS films during evaporation, a very slow evaporation rate (~ 0.1 nm/s) was used, with the SiO_x layers deposited as multiple repetitions of 6-nm-thick layers [17]. For each evaporation, SiO_x was also evaporated onto clean Si wafers for independent capping layer thickness determination using ellipsometry. The index of refraction of the SiO_x layers was consistent with $1 < x < 2$.

Following the deposition of the capping layers, the freely standing trilayer films were free from defects and uniform in color with no structure when viewed along

 0031-9007/99/82(7)/1486(4)$15.00 © 1999 The American Physical Society

the film normal with optical microscopy. Wrinkles in the trilayer films were observed, produced by expansion of the PS film during SiO_x evaporation due to minor heating. Upon cooling to room temperature, the SiO_x films do not contract as much as the PS film so that the trilayer film has a larger surface area than that of the initial PS film.

The trilayer films were annealed under vacuum at 210 °C for 3 h. This is a very high temperature for PS, well above the glass transition temperature $T_g = 97 \pm 2$ °C, but less than that at which degradation of the PS molecules occurs [18]. If uncapped freely standing PS films were heated to this temperature, they would quickly self-destruct due to spontaneous hole formation [11]. Although rupture of the freely standing trilayer films does not occur, the annealing procedure produces a novel lateral morphology which forms and remains unchanged after ~1 h at $T = 210$ °C. We note that the annealing procedure, for long times at high temperature, removes any stress produced within the trilayer films during sample preparation. The final morphology is studied using reflected-light microscopy.

Figure 1a shows a typical optical microscope image obtained for an annealed freely standing SiO_x-PS-SiO_x trilayer film. The morphology of the annealed films is very distinctive: many long, parallel domains with well-defined characteristic periodicity. To determine the wavelength of the periodicity, we performed a numerical two-dimensional fast Fourier transform (FFT) on gray scale images corresponding to sample areas that were 50 times larger than that shown in Fig. 1a. The larger images contained many smaller regions such as that shown in Fig. 1a, each with a well-defined direction for the domains, with a random orientation of the different regions. The corresponding FFT of the larger image for the same trilayer film (inset of Fig. 1b) consists of a ring in reciprocal space. We average the intensity of the FFT tangential to the ring, and fit the average intensity versus reciprocal dimension to the contrast transfer function (background) of the microscope and a Gaussian signal peak (see Fig. 1b). From the reciprocal dimension corresponding to the maximum intensity of the Gaussian peak, we obtain the characteristic wavelength λ_{expt} that we associate with the morphology of the sample.

The observed morphology can be understood qualitatively by considering the different contributions to the change in the free energy. With the deformation of the capping layers, there is a decrease in free energy due to the attractive, long-range dispersion interaction across the film thickness, and an increase in the free energy associated with the bending of the capping layers [19]. If the capping layers are sufficiently thin *and* the PS is sufficiently mobile (as it is when annealed at 210 °C), the overall energy is reduced by deforming the capping layers and squeezing the PS into domains. This produces a corrugation of the film surfaces and the associated lateral morphology, as shown schematically in Fig. 2b. Parallel domains are obtained because it requires less energy to deform a sheet (each capping layer) in parallel bends than in uncorrelated deformations.

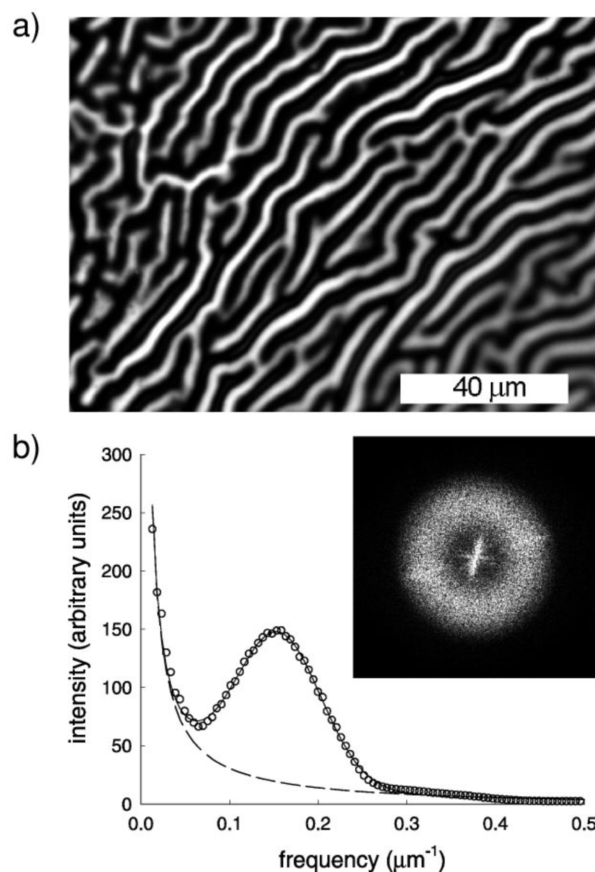

FIG. 1. (a) Optical microscope image obtained for an annealed SiO_x-PS-SiO_x film with $h = 121$ nm and $L = 22$ nm. (b) Average intensity as a function of reciprocal dimension calculated from the fast Fourier transform shown in the inset. The fit (solid line) is a sum of a Gaussian signal peak and the contrast transfer function (dashed line) of the microscope.

The observed morphology can be understood quantitatively by considering a simple model of a fluid film symmetrically confined by solid layers. At the outset, we make a number of simplifying assumptions. First, we note that the largest contribution to the dispersion force comes from the capping layer-air interfaces where the optical index of refraction discontinuity is large [12]. Thus, for the calculation of the dispersion force, we ignore the fluid-capping layer interfaces within the trilayer film where the index discontinuity is small and treat the film as a single layer of continuous material. Second, we use only the nonretarded form of the dispersion force [12], as specified by the Hamaker constant. This is not rigorously true for the length scales relevant to the present calculation (~100 nm) but it is known to be a satisfactory approximation [9,12]. We also assume a sinusoidal deformation of the capping layers with wavelength λ, symmetric about the midplane of the fluid film, and the morphology is assumed to be described by parallel domains that extend infinitely along the long axis of the domains. For the purposes of understanding the origin of the morphology and

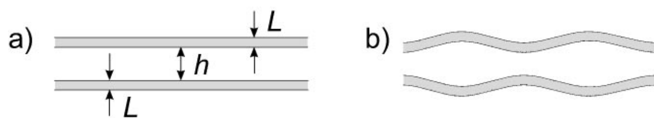

FIG. 2. Schematic diagrams of the cross section of a freely standing trilayer film (a) after deposition of the capping layers and (b) after annealing.

quantifying the scaling behavior of the morphology, the above assumptions are satisfactory.

We represent the displacement of the capping layer normal to the film plane at any point along the film cross section by ζ (positive away from the midplane of the film). The pressure within the fluid film has two contributions: the pressure P_D induced by the dispersion force which drives the morphology and the pressure P_B due to the bending of the capping layers. The pressure P on the fluid, after dropping the irrelevant constant $A/[6\pi(h + 2L)^3]$, can be written as [12,20]

$$P = P_B + P_D \approx \left[D(\nabla^2)^2 - \frac{A}{\pi(h + 2L)^4} \right] \zeta , \quad (1)$$

where $D = (EL^3)/[12(1 - \sigma^2)]$, E and σ are the Young's modulus and Poisson's ratio of the capping layer material, and A is the Hamaker constant associated with the capping layer-air interfaces.

The pressure gradient within the fluid film produces the flow of the fluid, squeezing the fluid out of the regions where the capping layer separation is decreased ($\zeta < 0$). We assume Poiseuille flow with no slippage at the fluid-capping layer boundaries. This simple fluid analysis is a useful first order approximation for a polymer melt at very high temperatures. The pressure gradient for the parabolic flow field is

$$-\vec{\nabla} P = \frac{2}{h} \times \text{edge stress} = \frac{2}{h} \eta \left. \frac{\partial \vec{v}}{\partial z} \right|_{\text{edge}} = \frac{8\eta}{h^2} \vec{v}_m , \quad (2)$$

where $\vec{v}$ is the fluid velocity, $\vec{v}_m$ is the maximum velocity obtained at the midplane of the fluid film, η is the viscosity, and the z direction is chosen normal to the film. Combining Eqs. (1) and (2) and the continuity equation which reduces to $\vec{\nabla} \cdot \vec{v}_m = -(3/h)(\partial \zeta / \partial t)$, we obtain

$$\frac{24\eta}{h^3} \frac{\partial \zeta}{\partial t} = \nabla^2 \left[D(\nabla^2 \zeta)^2 - \frac{A\zeta}{\pi(h + 2L)^4} \right] . \quad (3)$$

Now, assume that the capping layer deformation is of the form $\zeta \sim e^{t/\tau} \cos(qx)$ described by wave vector $\vec{q}$, with $q = 2\pi/\lambda$, and time constant τ. The x direction lies in the plane of the film and perpendicular to the long axis of the fluid domains. Substituting this form of the solution into Eq. (3), we obtain

$$\frac{1}{\tau} \frac{24\eta}{h^3} = -Dq^6 + \frac{Aq^2}{\pi(h + 2L)^4} . \quad (4)$$

There is exponential growth of the deformation for $q < q_c = \sqrt[4]{A/\pi D}\,(h + 2L)$. The wave vector that grows most rapidly is $q_m = q_c/\sqrt[4]{3}$, with corresponding wavelength

$$\lambda = 2\pi \sqrt[4]{\pi E/4A(1 - \sigma^2)}\, L^{3/4}(h + 2L) \quad (5)$$

which can be compared to the characteristic wavelength values λ_{expt} measured in the experiment.

From Eq. (5) it is clear that for a plot of $\lambda L^{-3/4}$ as a function of the trilayer film thickness $h + 2L$ all of the data should lie on a straight line. In Fig. 3 we show this plot for three different sets of trilayer films, each with a different capping layer thickness L. Within each set of films the PS film thickness h ranges from 31 nm to 121 nm. Clearly, the data is well described by the scaling behavior predicted by the model.

The slope of the best fit to the data in Fig. 3, $(2.7 \pm 0.4) \times 10^7$ m$^{-3/4}$, can be compared to the prefactor calculated in the model [Eq. (5)], using the elastic properties of fused quartz ($E = 72$ GPa, $\sigma = 0.16$ [21]) and the Hamaker constant for quartz-vacuum ($A = 6.5 \times 10^{-20}$ J [12]). The calculated prefactor is larger than the experimentally determined prefactor by a factor of 7. This discrepancy may be due to the simplifying assumptions and the approximation of the material properties of SiO_x as those of fused quartz. Perhaps more importantly, the energetics of the *final* lateral morphology can be quite different: The dispersion contribution increases dramatically as $h \rightarrow 0$ and, furthermore, when $h = 0$ interfacial energy terms must be included. These can be large, reducing the total free energy and driving λ to smaller values. Perhaps it is surprising that the length scale predicted by the linear model is modified by a fixed factor through the nonlinear development process. We emphasize that, as a description of the driving mechanism, the model must be correct since the transformation from lamellar to lateral morphology proceeds through the linear regime. As a result, the model will correctly predict the final outcome based on the sign of A.

There are only two requirements to obtain the lateral morphology from the simplified model presented above:

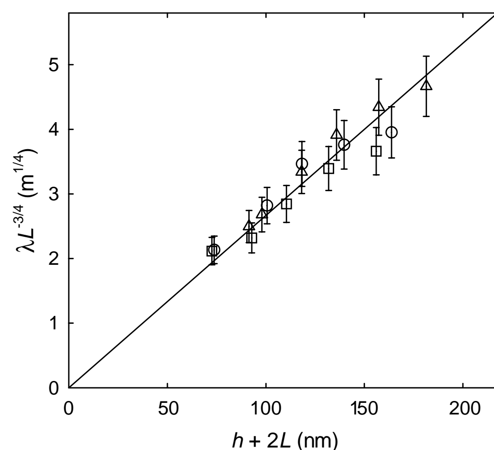

FIG. 3. Universal plot of $\lambda L^{-3/4}$ versus the trilayer film thickness $h + 2L$ for three series of samples with capping layer thicknesses $L = 17.7$ nm (□), 21.6 nm (○), and 30.4 nm (△).

The capping layers must be solid, but thin enough to allow deformation at a temperature for which the intermediate layer is in the melt phase; and the dispersion force must be attractive and large enough to drive the morphology. To test the general nature of these two requirements, we studied three other freely standing trilayer film systems containing different polymers and capping layer materials: SiO_x-PMMA-SiO_x, Au-PS-Au, and PS-PI-PS. PMMA is poly(methyl methacrylate) with $\overline{M}_w = 1221 \times 10^3$ and PI is polyisoprene with $\overline{M}_w = 414 \times 10^3$. The SiO_x and Au layers were evaporated onto freely standing polymer films. The PS-PI-PS films were made by spincoating a PI/PS bilayer film on a glass slide and subsequently depositing the final PS layer using a water transfer technique. For all freely standing trilayer films the same type of morphology was observed after annealing the films: parallel, elongated domains as in Fig. 1a.

The contributions to changes in the free energy included in the model imply that the same morphology may also be observed for capped films supported on a substrate. The main difference is the nature of the dispersion force for the asymmetric versus symmetric film geometry. The following systems were studied: Au-PS-SiO_2, SiO_x-PS-(Si-H), PS-PI-(Si-H), and PS-PI-(SiO_x-Si), where (Si-H) is hydrogen-terminated Si and (SiO_x-Si) is a 30 nm layer of SiO_x on Si. All of the samples exhibited the same type of lateral morphology as shown in Fig. 1 after annealing.

We have achieved *reversibility* of the morphology by manipulation of the dispersion force after the annealing of a PS-PI-PS freely standing trilayer film. When part of the annealed trilayer film with a lateral morphology was placed onto a Si wafer and subsequently annealed, we observed that the morphology for the supported region of the film reverted back to the lamellar structure (see Fig. 4). The reversion to the initial lamellar morphology occurs because the dispersion force is either reduced or repulsive by placing the film onto the Si wafer.

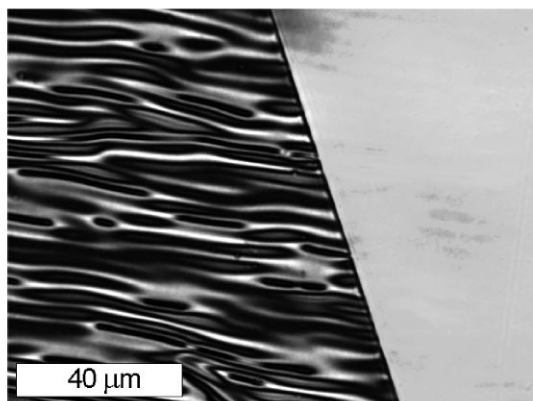

FIG. 4. Optical microscope image of a PS-PI-PS sample with $h = 50$ nm and $L = 70$ nm. The film is freely standing on the left side of the image, and the film is supported on a Si wafer on the right side of the image.

In summary, we have shown that mechanical confinement of thin polymer films can lead to a novel lateral morphology driven by the dispersion force. We have presented a simple model which describes the mechanism responsible for the morphology and the scaling behavior with film thickness. Eight different systems, both freely standing and supported films, were investigated and all exhibit the same type of lateral morphology upon annealing, illustrating the general nature of the mechanism. In one case it was shown that the morphology is reversible by manipulation of the dispersion force.

We thank Christian Gigault for performing the ellipsometry measurements. Financial support from the Natural Sciences and Engineering Research Council (NSERC) of Canada is gratefully acknowledged.

*To whom correspondence should be addressed

[1] J. A. Forrest, K. Dalnoki-Veress, and J. R. Dutcher, Phys. Rev. E **56**, 5705 (1997), and references therein.
[2] X. Zheng *et al.,* Phys. Rev. Lett. **79**, 241 (1997).
[3] E. K. Lin, W. Wu, and S. K. Satija, Macromolecules **30**,7224 (1997).
[4] A. N. Semenov, Phys. Rev. Lett. **80**, 1908 (1998).
[5] J. A. Forrest *et al.,* Phys. Rev. E **58**, R1226 (1998).
[6] K. Dalnoki-Veress, J. A. Forrest, and J. R. Dutcher, Phys. Rev. E **57**, 5811 (1998).
[7] C. Redon, F. Brochard-Wyart, and F. Rondelez, Phys. Rev. Lett. **66**, 715 (1991).
[8] G. Reiter, Phys. Rev. Lett. **68**, 75 (1992).
[9] F. Brochard-Wyart, P. Martin, and C. Redon, Langmuir **9**, 3682 (1993).
[10] G. Debrégeas, P. Martin, and F. Brochard-Wyart, Phys. Rev. Lett. **75**, 3886 (1995).
[11] K. Dalnoki-Veress, B. G. Nickel, C. Roth, and J. R. Dutcher, Phys. Rev. E (to be published).
[12] J. N. Israelachvili, *Intermolecular & Surface Forces* (Academic, San Diego, 1991), 2nd ed.
[13] W. R. McEntee and K. J. Mysels, J. Phys. Chem. **73**, 3018 (1969).
[14] A. Vrij, F. Th. Hesselink, J. Lucassen, and M. Van Den Tempel, Koninkl. Nederl. Academie van Wetenschappen Amsterdam B **73**, 124 (1970).
[15] A. C. Balazs *et al.,* MRS Bull. **22**, 16 (1997).
[16] P. Lambooy, J. R. Salem, and T. P. Russell, Thin Solid Films **252**, 75 (1994).
[17] Heating effects associated with the SiO_x evaporation are not important since we have observed quantitatively the same lateral morphology (see Fig. 1a) for evaporation rates of $\sim$0.2 nm/s.
[18] *Polymer Handbook,* edited by J. Brandrup and E. H. Immergut (Wiley, New York, 1989), 3rd ed.
[19] The change in free energy associated with the PS-SiO_x interfacial tension is very small because additional interface is not created in the annealing of the wrinkled films.
[20] L. D. Landau and E. M. Lifshitz, *Theory of Elasticity* (Pergamon, Oxford, 1986), 3rd ed., pp. 38–40.
[21] *CRC Handbook of Chemistry and Physics,* edited by D. R. Lide (CRC, Boca Raton, 1994), 75th ed.